3-D FIR Cone-Shaped Filter Design by a Nest of McClellan Transformations and Its Variable Design

Jong-Jy Shyu, *Member, IEEE*, Soo-Chang Pei, *Fellow, IEEE*, and Yun-Da Huang

***Abstract*—In this paper, the technique of a nest of McClellan transformations is proposed for the design of 3-D FIR cone-shaped filters. First, a transformation subfilter for fan-type mapping is found. Then the cosine term of a frequency variable of the above transformation subfilter is replaced by an embedded transformation subfilter which possesses circular contours. The technique stated above is also extended to design 3-D FIR variable cone-shaped filters such that the inclination of the cone-shaped filters can be adjusted online. Moreover, an efficient structure is proposed for the implementation of the designed filters. Several examples will be presented to demonstrate the effectiveness of the proposed method.**

***Index Terms*—Cone-shaped filter, finite-impulse-response (FIR) filter, three-dimensional (3-D) filter, McClellan transformation, variable filter, least-squares method.**

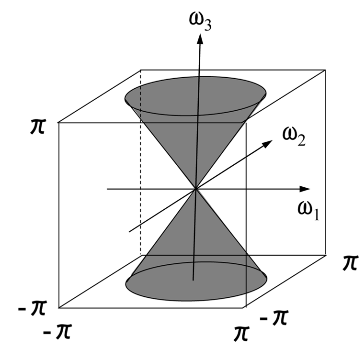

Fig. 1. Ideal cone shape for designing a 3-D cone-shaped filter. (Shadowy region: passband).

I. Introduction

FOR designing a 3-D cone-shaped filter, the ideal cone shape, which is illustrated in Fig. 1, can be described by

$$\omega_1^2+\omega_2^2=\frac{\omega_3^2}{\tan^2(\theta)} \tag{1}$$

where θ denotes the angle between the cone-surface and the (ω_1,ω_2)-plane. Recently, the design of 3-D cone-shaped filters has received considerable attention due to their wide applications in areas such as processing of geological and seismological data, sonar and radar engineering, and motion discrimination [1]–[15]. Among the existing literature, it is impressive for [12], [13] and [15] in which the technique of McClellan transformation is applied to the design of 3-D FIR cone-shaped filters.

In the design of 2-D FIR digital filters, McClellan transformation plays a dominant role [16]–[30]. Applying the technique, a high-order 1-D prototype filter and a low-order 2-D transformation subfilter are designed, respectively, then the 1-D prototype filter is mapped into a 2-D filter by a change of variables.

In this paper, the design of 3-D FIR cone-shaped filters is investigated by a nest of McClellan transformations. First, a 2-D FIR fan-type filter with inclination θ is designed by McClellan transformation and the following substitution is used:

$$\begin{aligned}\cos(\omega)\\ &=t_{00}+t_{10}\cos(\omega_{12})+t_{01}\cos(\omega_3)+t_{11}\cos(\omega_{12})\cos(\omega_3)\end{aligned} \tag{2}$$

The design specification is illustrated in Fig. 2(a). Then, the term $\cos(\omega_{12})$ in (2) is replaced by

$$\begin{aligned}\cos(\omega_{12})\\ &=r_{00}+r_{10}\cos(\omega_1)+r_{01}\cos(\omega_2)+r_{11}\cos(\omega_1)\cos(\omega_2)\end{aligned} \tag{3}$$

and the circular cutoff contour shown in Fig. 2(b) is required to meet an ideal one as much as possible. To find the coefficients in (2) and (3), some constraints are incorporated in this paper such that scaling problem can be avoided. Although higher order transformation subfilters in (2) and (3) can be used for accuracy, the complexity of the designed system will increase drastically. So, only first-order transformation subfilters are adopted in this paper.

Also, there is another trend of filter design concerning the design of variable filters which are applied applications where the frequency characteristics need to be adjustable [31]–[42]. Among the existing works, especially, the technique of McClellan transformation is applied in [40]–[42] to the design of 2-D FIR variable filters. In this paper, it will be dealt with for the design of 3-D FIR variable cone-shaped filters by a nest of variable McClellan transformations.

This paper is organized as follows. In Section II, the technique of a nest of McClellan transformations is applied to the design of 3-D FIR cone-shaped filters, which will be extended to the design of 3-D FIR variable cone-shaped filters in Section III. Several examples will be presented to demonstrate the effectiveness of the proposed method. Finally, the conclusions will be given in Section IV.

Manuscript received May 28, 2009; revised July 25, 2009; accepted September 01, 2009. Date of publication December 28, 2009; date of current version July 16, 2010. This work was supported by the National Science Council, Taiwan, under Grants NSC 98-2221-E-390-019. This paper was recommended by Y.-P. Lin.

J.-J. Shyu is with the Department of Electrical Engineering, National University of Kaohsiung, Kaohsiung, Taiwan (e-mail: jshyu@nuk.edu.tw).

S.-C. Pei and Y.-D. Huang are with the Graduate Institute of Communication Engineering, National Taiwan University, Taipei, Taiwan (e-mail: pei@cc.ee.ntu.edu.tw, d97942016@ntu.edu.tw).

Digital Object Identifier 10.1109/TCSI.2009.2033547

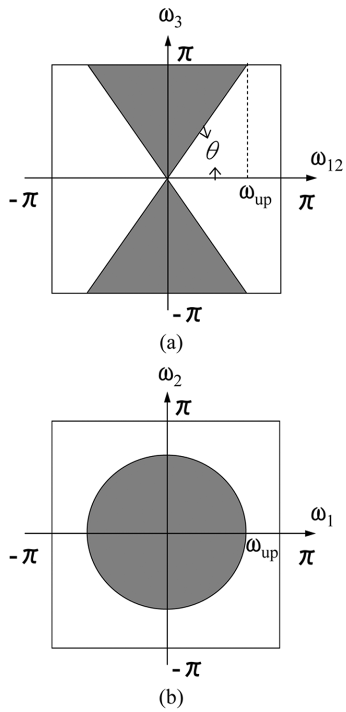

Fig. 2. (a) Specification for the design of a fan-type filter. (b) Circular cutoff contour for the embedded transformation of the proposed method. (Shadow regions: passbands).

II. Design of 3-D FIR Cone-Shaped Filters by a Nest of McClellan Transformations

For a zero-phase FIR digital filter, its frequency response can be represented by

$$H(\omega)=\sum_{n=0}^{N} a_n \cos(n\omega). \tag{4}$$

Replacing $\cos(n\omega)$ in (4) by the nth-order Chebyshev polynomial, (4) becomes

$$H(\omega)=\sum_{n=0}^{N} a_n T_n[\cos(\omega)]. \tag{5}$$

Generally, for designing a 3-D FIR digital filter by McClellan transformation the substitution shown below is used

$$\begin{aligned}\cos(\omega) =& F(\omega_1,\omega_2,\omega_3)\\ =& t_{000}+t_{100}\cos(\omega_1)\\ &+t_{010}\cos(\omega_2)+t_{001}\cos(\omega_3)\\ &+t_{110}\cos(\omega_1)\cos(\omega_2)+t_{101}\cos(\omega_1)\cos(\omega_3)\\ &+t_{011}\cos(\omega_2)\cos(\omega_3)+t_{111}\cos(\omega_1)\cos(\omega_2)\cos(\omega_3)\end{aligned} \tag{6}$$

and the frequency response of the designed 3-D FIR filter is

$$H(\omega_1,\omega_2,\omega_3)=\sum_{n=0}^{N} a_n T_n[F(\omega_1,\omega_2,\omega_3)]. \tag{7}$$

For the Chebyshev polynomial, there exist the following recurrence relations.

$$T_0(x)=1 \tag{8a}$$
$$T_1(x)=x \tag{8b}$$
$$T_n(x)=2xT_{n-1}(x)-T_{n-2}(x) \tag{8c}$$

hence the system with the frequency response in (7) can be implemented by the structure shown in Fig. 3(a) where $F(z_1,z_2,z_3)$ is the corresponding transfer function of (6), which can be obtained by replacing $\cos(\omega_i)$ by $(z_i+z_i^{-1})/2$, $i=1,2,3$.

In this section, the technique of a nest of McClellan transformations is applied. First, a 2-D transformation subfilter for designing a 2-D fan-type filter with inclination θ is achieved by the substitution (2), and it is desirable that the cutoff contour shown in Fig. 2(a) can be met as much as possible. In Fig. 2(a),

$$\omega_{\rm up}=\begin{cases}\pi, & \text{if } \theta\le 45^\circ,\\ \pi/\tan(\theta), & \text{if } \theta>45^\circ.\end{cases} \tag{9}$$

Once the coefficients in (2) are determined, the second transformation for circular contour mapping is proceeded by replacing $\cos(\omega_{12})$ in (2) by (3). Hence, (2) becomes

$$\begin{aligned}\cos(\omega)=&\, t_{00}+t_{10}r_{00}+t_{10}r_{10}\cos(\omega_1)+t_{10}r_{01}\cos(\omega_2)\\ &+(t_{01}+t_{11}r_{00})\cos(\omega_3)+t_{10}r_{11}\cos(\omega_1)\cos(\omega_2)\\ &+t_{11}r_{10}\cos(\omega_1)\cos(\omega_3)+t_{11}r_{01}\cos(\omega_2)\cos(\omega_3)\\ &+t_{11}r_{11}\cos(\omega_1)\cos(\omega_2)\cos(\omega_3).\end{aligned} \tag{10}$$

Comparing (6) and (10), the relationships shown below can be obtained

$$\begin{cases} t_{000}=t_{00}+t_{10}r_{00}\\ t_{100}=t_{10}r_{10}\\ t_{010}=t_{10}r_{01}\\ t_{001}=t_{01}+t_{11}r_{00}\\ t_{110}=t_{10}r_{11}\\ t_{101}=t_{11}r_{10}\\ t_{011}=t_{11}r_{01}\\ t_{111}=t_{11}r_{11}.\end{cases} \tag{11}$$

A. Determination of the Transformation Coefficients in (2)

To find the transformation coefficients in (2), it is desirable to incorporate the following constraints such that scaling problem can be avoided: (1) The 1-D frequency origin, $\omega=0$, is mapped into the $(\omega_{12},\omega_3)=(0,\pi)$ point of the 2-D frequency plane, and (2) the point $\omega=\pi$ is mapped into $(\omega_{12},\omega_3)=(\pi,0)$, which leads to

$$t_{00}=t_{11} \tag{12a}$$
$$t_{10}=1+t_{01}. \tag{12b}$$

Moreover, $\omega_3=\omega_{12}\tan(\theta)$ along the cutoff contour shown in Fig. 2(a), so the objective error function can be represented by the following:

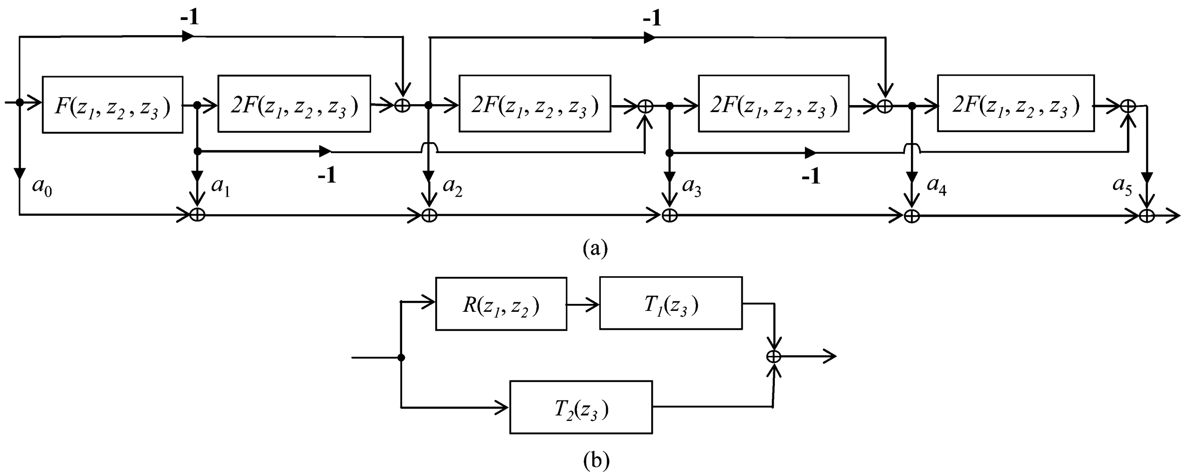

Fig. 3. (a) Structure of a 3-D FIR filter designed by McClellan transformation ($N = 5$). (b) Block diagram of the transformation subfilter designed by the proposed method.

$$
\begin{aligned}
e(\mathbf{t}) &= \int_0^{\omega_{\rm up}} [\cos(\omega_c) - \cos(\omega_{12}) - t_{11}(1+\cos(\omega_{12})\cos(\omega_3)) \\
&\quad - t_{01}(\cos(\omega_{12})+\cos(\omega_3))]^2 d\omega_{12} \\
&= \int_0^{\omega_{\rm up}} [\cos(\omega_c) - \cos(\omega_{12}) - \mathbf{t}^T\mathbf{c}(\omega_{12})]^2\, d\omega_{12} \\
&= s_f + \mathbf{t}^T\mathbf{r}_f + \mathbf{t}^T\mathbf{Q}_f\mathbf{t}
\end{aligned} \tag{13}
$$

where ω_c is the cutoff frequency of 1-D prototype filter, the superscript^T denotes the transposed operator,

$$\mathbf{t} = [t_{11}, t_{01}]^T \tag{14a}$$

$$
\begin{aligned}
\mathbf{c}(\omega_{12}) = [&1+\cos(\omega_{12})\cos(\omega_{12}\tan(\theta))\cos(\omega_{12}) \\
&+\cos(\omega_{12}\tan(\theta))]^T
\end{aligned} \tag{14b}
$$

$$s_f = \int_0^{\omega_{\rm up}} [\cos(\omega_c) - \cos(\omega_{12})]^2 d\omega_{12} \tag{14c}$$

$$\mathbf{r}_f = -2\int_0^{\omega_{\rm up}} [\cos(\omega_c) - \cos(\omega_{12})]\mathbf{c}(\omega_{12}) d\omega_{12} \tag{14d}$$

$$\mathbf{Q}_f = \int_0^{\omega_{\rm up}} \mathbf{c}(\omega_{12})\mathbf{c}^T(\omega_{12}) d\omega_{12}. \tag{14e}$$

For a given ω_c, the minimum of (13) can be obtained by differentiating $e(\mathbf{t})$ with respect to $\mathbf{t}$ and setting the result to zero, which yields

$$\mathbf{t} = -\frac{1}{2}\mathbf{Q}_f^{-1}\mathbf{r}_f. \tag{15}$$

To determine the cutoff frequency of 1-D prototype filter, the error curve of $e(\mathbf{t})$ for $0 \le \omega_c \le \pi$ can be obtained and the corresponding ω_c with the minimum error is the desired one.

When $\theta = 65^\circ$ and the step size $\Delta = \pi/10^5$ is used, for example, the error curve of $e(\mathbf{t})$ is shown in Fig. 4(a), the cutoff frequency of 1-D prototype filter is $\omega_c = 0.24776\pi, t_{11} = 0.25145973, t_{01} = -0.39113345$ and the isopotential contours are illustrated in Fig. 4(b) where the values inside the figure represent the frequencies of prototype low-pass filter.

B. *Design of 1-D Prototype Filters*

In this section, the 1-D prototype low-pass FIR filter is designed by the Remez exchange algorithm [43]. For example, when $N = 20$, passband $[0, \omega_c = 0.24776\pi]$, stopband $[\omega_c + 0.1\pi, \pi]$, the magnitude response is shown in Fig. 4(c).

C. *Determination of the Transformation Coefficients in (3)*

For deriving the coefficients in (3), three constraints are considered: (1) $\omega_{12} = 0$ is mapped into $(\omega_1,\omega_2) = (0,0)$, (2) $\omega_{12} = \pi$ is mapped into $(\omega_1,\omega_2) = (\pi,\pi)$, and (3) $r_{01} = r_{10}$ due to symmetry, which leads to

$$r_{00} = -r_{11} \tag{16a}$$

$$r_{01} = r_{10} = 1/2. \tag{16b}$$

Hence the corresponding objective error function can be represented by

$$
\begin{aligned}
e(r_{11}) &= \int_c \Bigg[\cos(\omega_{12c}) - \frac{1}{2}\cos(\omega_1) - \frac{1}{2}\cos(\omega_2) \\
&\qquad + r_{11} - r_{11}\cos(\omega_1)\cos(\omega_2)\Bigg]^2 dl \\
&= s_c + r_{11}r_c + r_{11}q_c^2
\end{aligned} \tag{17}
$$

where $\int_c \cdot dl$ denotes a line integral along the circular cutoff contour shown in Fig. 2(b)

$$s_c = \int_c \left[\cos(\omega_{12c}) - \frac{1}{2}\cos(\omega_1) - \frac{1}{2}\cos(\omega_2)\right]^2 dl \tag{18a}$$

$$
\begin{aligned}
r_c = -2\int_c &\left[\cos(\omega_{12c}) - \frac{1}{2}\cos(\omega_1) - \frac{1}{2}\cos(\omega_2)\right] \\
&\times [\cos(\omega_1)\cos(\omega_2) - 1] dl
\end{aligned} \tag{18b}
$$

$$q_c = \int_c [\cos(\omega_1)\cos(\omega_2) - 1]^2 dl. \tag{18c}$$

Obviously, for a given ω_{12c}, the minimum of (17) is obtained for $r_{11} = -r_c/(2q_c)$. Also the proper frequency point ω_{12c}, which is mapped into the circular cutoff contour shown in Fig. 2(b), must be determined by choosing the frequency ω_{12c} where $e(r_{11})$ is minimum. For example, when $\theta = 65^\circ$ and

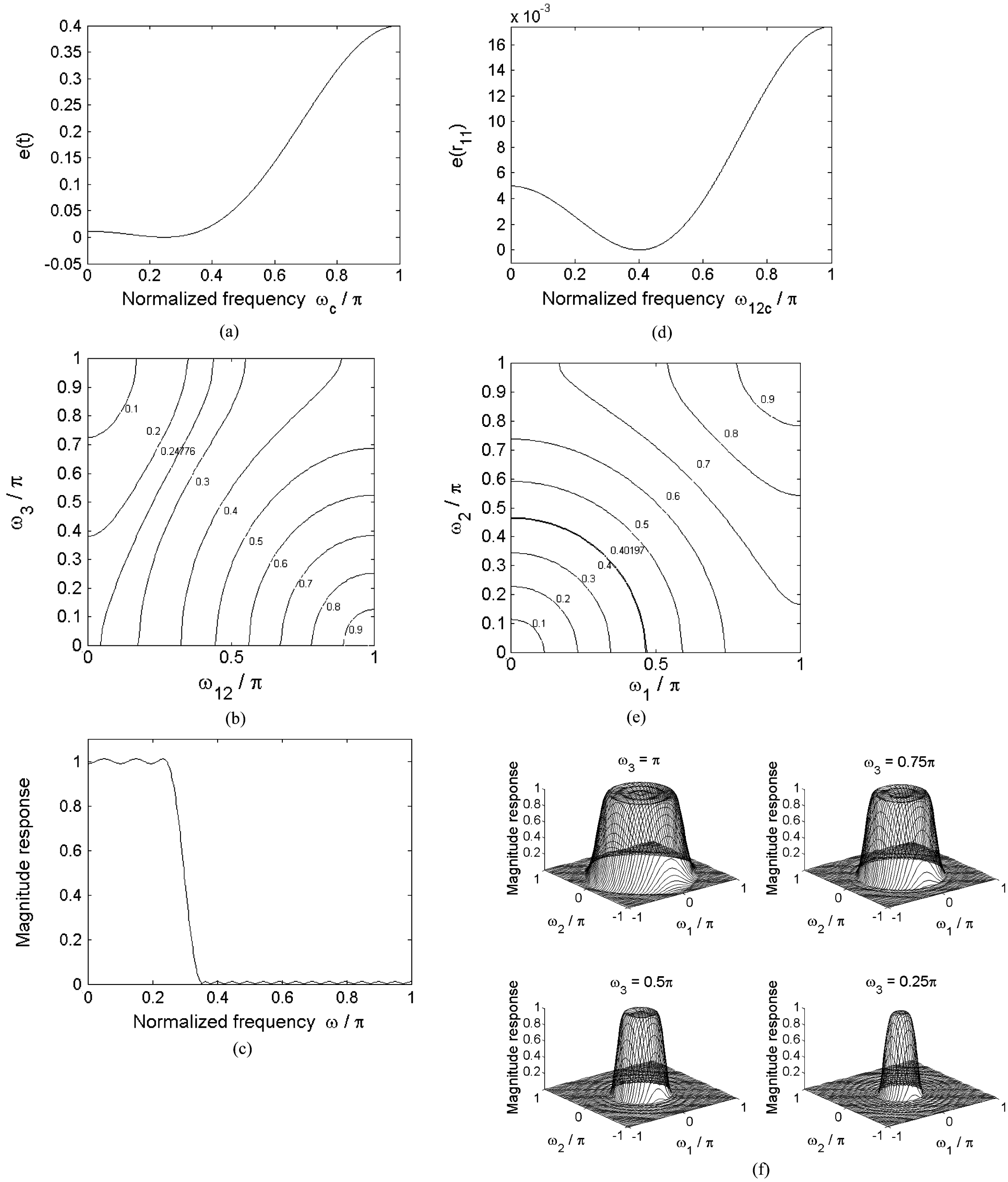

Fig. 4. Design of a 3-D FIR cone-shaped filter with $\theta = 65^\circ$ and $N = 20$. (a) Error curve for fan-type contour fitting. (b) Isopotential contours for fan-type contour fitting. (c) Magnitude response of 1-D FIR prototype filter. (d) Error curve for circular contour fitting. (e) Isopotential contours for circular contour fitting. (f) Magnitude responses of the designed cone-shaped filter for $\omega_3 = \pi, 0.75\pi, 0.5\pi$, and 0.25π.

$\Delta = \pi/10^5, \omega_{\rm up} = \pi/\tan(65^\circ)$, the error curve $e(r_{11})$ for $0 \le \omega_{12c} \le \pi$ is shown in Fig. 4(d), the desired ω_{12c} is $0.40197\pi, r_{11} = 0.27917598$, and the isopotential contours are illustrated in Fig. 4(e) where the values inside the figure represent the frequencies ω_{12} of the fan-type filter designed in Section II-A.

D. Derivation of the Filter Coefficients for the 3-D Cone-Shaped Filter

Substituting (3) into (2), the transfer function of the transformation subfilter can be represented by

$$\begin{aligned} F(z_1, z_2, z_3) &= \left(r_{00} + r_{10}\frac{z_1 + z_1^{-1}}{2} + r_{01}\frac{z_2 + z_2^{-1}}{2} \right. \\ &\quad \left. + r_{11}\frac{z_1 + z_1^{-1}}{2}\frac{z_2 + z_2^{-1}}{2}\right) \\ &\quad \cdot \left(t_{10} + t_{11}\frac{z_3 + z_3^{-1}}{2}\right) + \left(t_{00} + t_{01}\frac{z_3 + z_3^{-1}}{2}\right) \end{aligned} \tag{19}$$

which will further become

$$F(z_1, z_2, z_3) = R(z_1, z_2)T_1(z_3) + T_2(z_3) \tag{20}$$

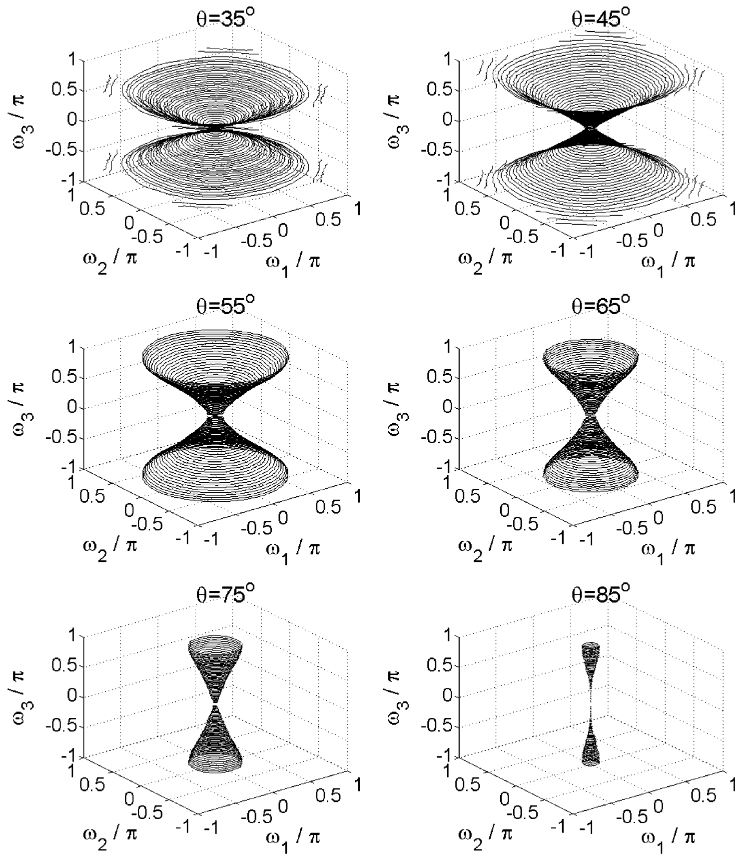

Fig. 5. Isopotential surfaces of 3-D FIR cone-shaped filters at magnitude 0.98 when $\theta = 35°, 45°, 55°, 65°, 75°$, and $85°$.

by incorporating the constraints in (12) and (16), where

$$R(z_1,z_2) = -r_{11} + \frac{z_1+z_1^{-1}}{4} + \frac{z_2+z_2^{-1}}{4} + r_{11}\frac{\left(z_1+z_1^{-1}\right)\left(z_2+z_2^{-1}\right)}{4} \quad \text{(21a)}$$

$$T_1(z_3) = 1 + t_{01} + t_{11}\frac{z_3+z_3^{-1}}{2} \quad \text{(21b)}$$

$$T_2(z_3) = t_{11} + t_{01}\frac{z_3+z_3^{-1}}{2} \quad \text{(21c)}$$

Hence, the original 3-D transformation subfilter can be simplified and implemented by the block diagram shown in Fig. 3(b), and it is easy to get the impulse response corresponding to the transfer function (20). By (5), (7) and (20), the resultant transfer function of the designed 3-D cone-shaped filter can be represented by

$$H(z_1,z_2,z_3) = \sum_{n=0}^{N} a_n T_n[F(z_1,z_2,z_3)] = \sum_{n=0}^{N} b_n F^n(z_1,z_2,z_3) \quad (22)$$

where b_n can be obtained from a_n by decomposing the recurrence relations in (8), and the filter coefficients can be obtained by the convolution method. For example, Fig. 4(f) presents magnitude responses for $\omega_3 = \pi, 0.75\pi, 0.5\pi$ and 0.25π when $\theta = 65°$ and the designed 1-D prototype low-pass FIR filter in Section II-B is applied, while the isopotential surface at magnitude 0.98 is shown in Fig. 5.

E. Comparisons and Discussions

To demonstrate the effectiveness of the proposed method, the results for $35° \leq \theta \leq 85°$ are tabulated in Table I, and the isopotential surfaces at magnitude 0.98 for $\theta = 35°, 45°, 55°, 65°, 75°$ and $85°$ are presented in Fig. 5 where the 1-D prototype filter is designed with $N = 20$, passband $[0, \omega_c]$, and stopband $[\omega_c + 0.1\pi, \pi]$. For comparing with the works in [12] and [15], the root-mean-squared deviation error of the cutoff isopotential is defined by

$$\varepsilon_{\rm rms} = \left\{ \frac{1}{(N_3+1)(N_{12}+1)} \times \sum_{n_3=0}^{N_3}\sum_{n_{12}=0}^{N_{12}} [\cos(\omega_c) - F(\omega_1,\omega_2,\omega_3)]^2 \right\}^{\frac{1}{2}}$$
$$\omega_3 = \begin{cases} n_3\pi/N_3, & \text{for } \theta \geq 45° \\ n_3\pi\tan(\theta)/N_3, & \text{for } \theta < 45° \end{cases}$$
$$\omega_1 = \frac{\omega_3}{\tan(\theta)}\cos\left(\frac{n_{12}\pi}{2N_{12}}\right)$$
$$\omega_2 = \frac{\omega_3}{\tan(\theta)}\sin\left(\frac{n_{12}\pi}{2N_{12}}\right) \quad (23)$$

and the results are also list in Table I when $N_{12} = N_3 = 90$. To peer the detail, the root-mean-squared deviation errors of the cutoff isopotentials, $\varepsilon_{\rm rms}$, for the proposed method and the methods in [12] and [15] are illustrated in Fig. 6. It can be observed from Table I and Fig. 6 that the proposed method and the methods in [12] and [15] own their respective feature: the overall

TABLE I
THE RELATED RESULTS FOR THE DESIGN OF 3-D FIR CONE-SHAPED FILTERS WITH $N = 20$ AND $35^\circ \le \theta \le 85^\circ$, AND COMPARISONS BETWEEN THE PROPOSED METHOD AND THE METHODS IN [12] AND [15]

θ	Proposed method						Method in [12]	Method in [15]
	ω_c/π	ω_{12c}/π	t_{11}	t_{01}	r_{11}	ε_{rms}	ε_{rms}	ε_{rms}
35°	0.63976	0.85269	-0.16348359	-0.5549171	0.44297755	0.04235498	0.11642287	0.07393103
40°	0.57545	0.85269	-0.09630886	-0.52574996	0.44297755	0.04618366	0.11146387	0.06861684
45°	0.5	0.85269	0	-0.5	0.44297755	0.04471952	0.09439354	0.09243811
50°	0.42455	0.71586	0.09630886	-0.47425004	0.36680456	0.06662341	0.03950643	0.0989269
55°	0.36024	0.59994	0.16348359	-0.4450829	0.32372541	0.06460113	0.07504389	0.10154284
60°	0.30212	0.49641	0.21333164	-0.4167224	0.29687193	0.05369084	0.08328548	0.09286125
65°	0.24776	0.40197	0.25145973	-0.39113345	0.27917598	0.04014389	0.07245512	0.07556123
70°	0.19585	0.31433	0.28066806	-0.36937651	0.26718397	0.0269322	0.05332988	0.05418291
75°	0.14561	0.2317	0.30240491	-0.3520417	0.25907298	0.01562093	0.0328281	0.03300801
80°	0.0965	0.15261	0.31746243	-0.33945032	0.25392453	0.00707627	0.01544117	0.01546517
85°	0.04808	0.07576	0.32636838	-0.3318541	0.25103676	0.00178751	0.00398336	0.00398445

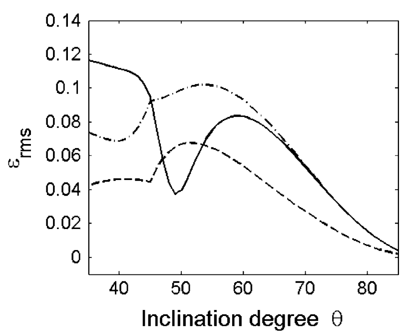

Fig. 6. The root-mean-squared deviation errors of the cutoff isopotentials. (Dash line: the proposed method, solid line: method of [12], dash-dot line: method of [15]).

performance of the proposed method is better while the others give uniform and closed-form solutions. It is noted that the performance of [12] is particularly better when $47^\circ \le \theta \le 53^\circ$.

As to the computation time, Matlab simulations show that each design took about 35.12 seconds in average on a notebook PC with Intel Core Duo CPU T8300. But if the step size Δ for finding the error curves in Fig. 4(a) and (d) is increased to $\pi/10^3$, the design only took 0.358 seconds of CPU time.

For the scaling problem of transformation function (10), exhaustive experiments show that the values of (10) for $\omega_i \in [-\pi, \pi], i = 1, 2, 3$ always lie inside $[-1, 1]$ when the constraints in (12) and (16) are considered in the design procedure.

III. Design of 3-D FIR Variable Cone-Shaped Filters

For designing a 3-D FIR variable cone-shaped filter with adjustable θ, the frequency response of the prototype filter is

$$H(\omega) = \sum_{n=0}^{N} a_n(p)\cos(n\omega) \tag{24}$$

where the adjustable variable is defined by

$$p = \tan(\theta) \tag{25}$$

and the coefficients $a_n(p)$ are expressed as the polynomials of p

$$a_n(p) = \sum_{m=0}^{M} a(n, m)p^m. \tag{26}$$

Similarly, the variable-type transformation subfilter of (20) is used and given by

$$F(z_1, z_2, z_3, p) = R(z_1, z_2, p)T_1(z_3, p) + T_2(z_3, p) \tag{27}$$

where

$$R(z_1, z_2, p) = -r_{11}(p) + \frac{z_1 + z_1^{-1}}{4} + \frac{z_2 + z_2^{-1}}{4} + r_{11}(p)\frac{(z_1 + z_1^{-1})(z_2 + z_2^{-1})}{4} \tag{28a}$$

$$T_1(z_3, p) = 1 + t_{01}(p) + t_{11}(p)\frac{z_3 + z_3^{-1}}{2} \tag{28b}$$

$$T_2(z_3, p) = t_{11}(p) + t_{01}(p)\frac{z_3 + z_3^{-1}}{2} \tag{28c}$$

and the transfer function of the designed variable system can be represented by

$$H(z_1, z_2, z_3) = \sum_{n=0}^{N} a_n(p)T_n[F(z_1, z_2, z_3, p)] \tag{29}$$

which can be implemented by the structure shown in Fig. 7(a). Following Fig. 3(b), the block diagram of the variable transformation subfilter is given in Fig. 7(b) where

$$\begin{cases} t_{11}(p) = \sum_{m=0}^{M} t(1, 1, m)p^m \\ t_{01}(p) = \sum_{m=0}^{M} t(0, 1, m)p^m \\ r_{11}(p) = \sum_{m=0}^{M} r(1, 1, m)p^m \end{cases} \tag{30}$$

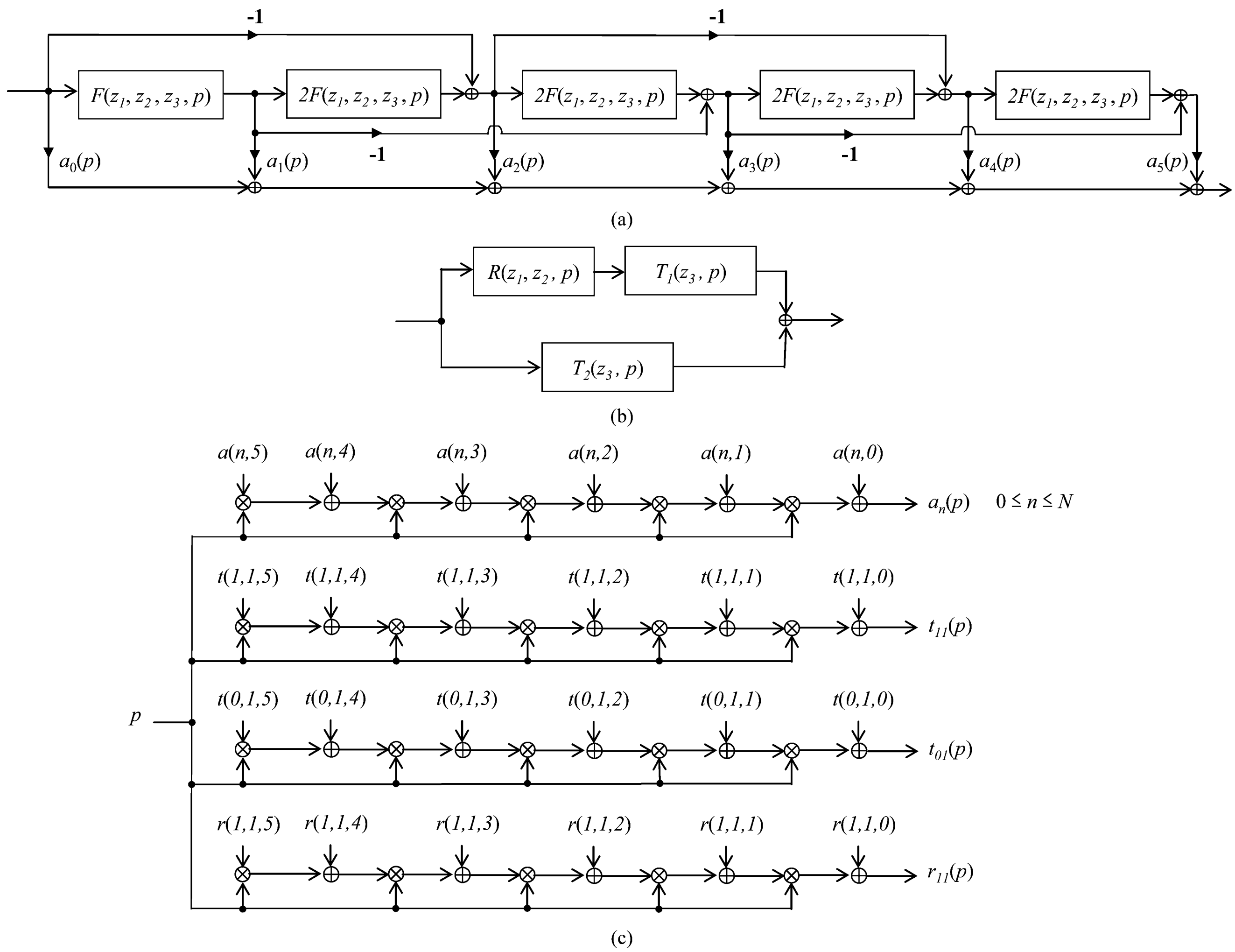

Fig. 7. (a) Structure of a 3-D FIR variable filter designed by variable McClellan transformation ($N = 5$). (b) Block diagram of the variable transformation subfilter designed by the proposed method. (c) Coefficient generators for the 1-D prototype filter and the transformation subfilter ($M = 5$).

and the coefficient generators for both the prototype 1-D filter and the transformation subfilter are shown in Fig. 7(c). It is noted that the coefficient generators are implemented such that the coefficients are changed only on the demand of variation.

A. Design of the Fan-Type Variable Transformation Subfilter and the 1-D Prototype Variable Filter

By (2) and (12), the substitution for the fan-type contour mapping can be represented by

$$\cos(\omega) = t_{11}(p)(1 + \cos(\omega_{12})\cos(\omega_3)) + t_{01}(p)(\cos(\omega_{12}) + \cos(\omega_3)) + \cos(\omega_{12}). \quad (31)$$

and the technique in [42] can be applied for the design of the fan-type variable transformation subfilter and the 1-D prototype variable filter, where a cutoff-frequency orbit function shown below must be determined

$$\omega_c(p) = b_0 + b_1 p + b_2 p^2 + \cdots + b_M p^M. \quad (32)$$

For example, it is desirable that θ is adjustable over $[\theta_1 = 55^\circ, \theta_2 = 75^\circ]$, so the variable range for parameter p is $[p_1 = \tan(\theta_1), p_2 = \tan(\theta_2)]$. When $M = 5$ is used, Fig. 8(a) shows the cutoff-frequency orbit accompanying the individual design with integer inclination angles in the range of $55^\circ \le \theta \le 75^\circ$ marked by "$\circ$", and the isopotential cutoff edge contours for different integer inclination degrees are shown in Fig. 8(b). The related coefficients are tabulated in Table II. For the design of 1-D prototype variable low-pass filter, the magnitude response is shown in Fig. 8(c) when $N = 20$ and the width of transition band $\omega_T = 0.15\pi$.

B. Design of the Circular-Type Variable Transformation Subfilter

By (3) and (16), the transformation for the circular-type contour mapping is

$$\cos(\omega_{12}) = r_{11}(p)(\cos(\omega_1)\cos(\omega_2) - 1) + \frac{1}{2}\cos(\omega_1) + \frac{1}{2}\cos(\omega_2). \quad (33)$$

To find the corresponding cutoff-frequency orbit function as

$$\omega_{12}(p) = \hat{b}_0 + \hat{b}_1 p + \hat{b}_2 p^2 + \cdots + \hat{b}_M p^M \quad (34)$$

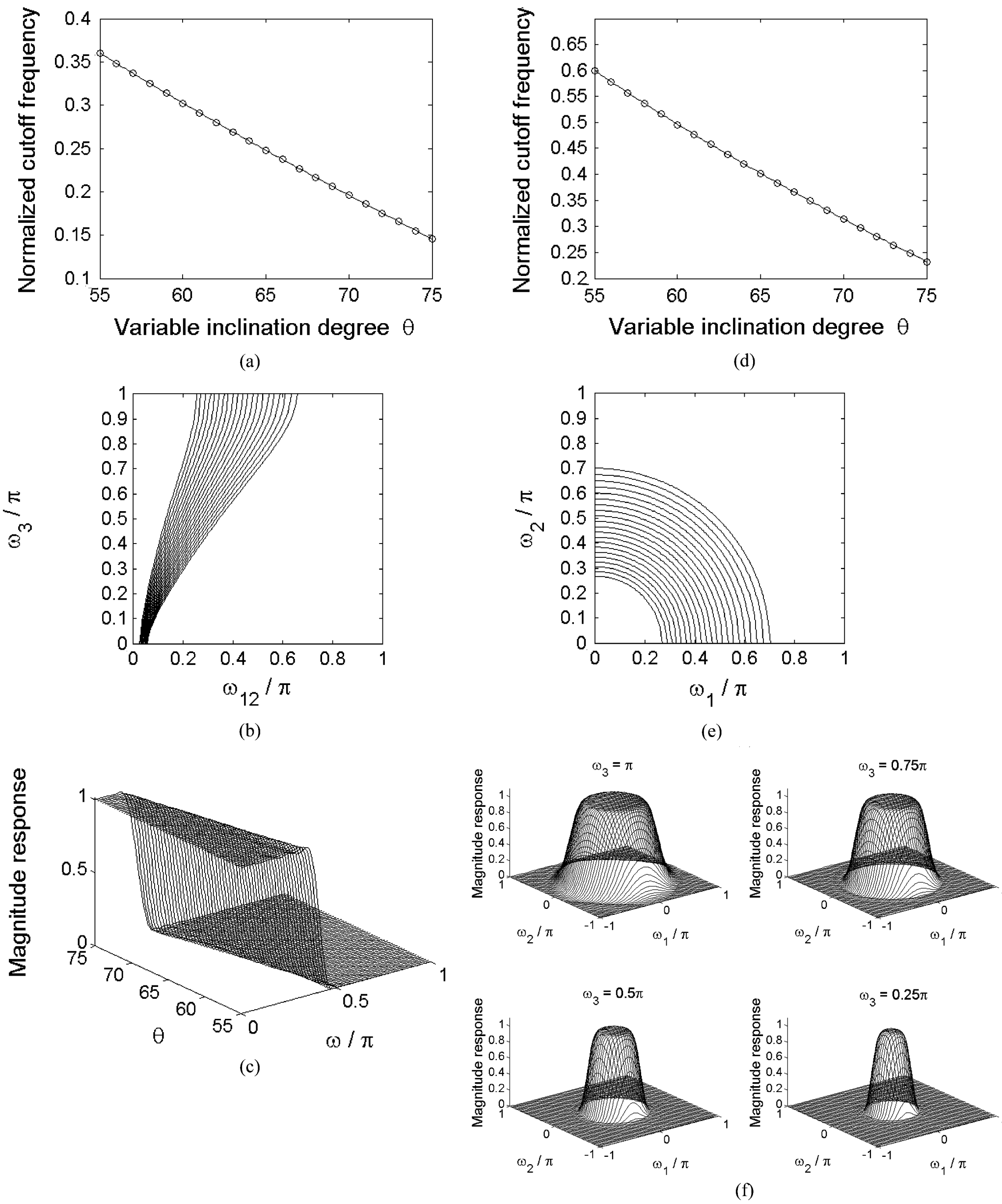

Fig. 8. Design of a 3-D FIR variable cone-shaped filter with $\theta_1 = 55°, \theta_2 = 75°, M = 5$ and $N = 20$. (a) Cutoff-frequency orbit for fan-type contour mapping. (b) Isopotential fan-type cutoff edge contours for different integer inclination degrees. (c) Magnitude response of the 1-D prototype variable low-pass filter. (d) Orbit of $\omega_{12}(p)$ for circular contour mapping. (e) Isopotential circular contours for different integer inclination degrees. (f) Magnitude responses for $\omega_3 = \pi, 0.75\pi, 0.5\pi$ and 0.25π when $\theta = 70°$.

it is necessary to solve the corresponding overdetermined system [44]

$$\begin{bmatrix} 1 & \tan(\theta_1) & \tan^2(\theta_1) & \cdots & \tan^M(\theta_1) \\ 1 & \tan(\theta_1+1) & \tan^2(\theta_1+1) & \cdots & \tan^M(\theta_1+1) \\ \vdots & \vdots & \vdots & \ddots & \vdots \\ 1 & \tan(\theta_2) & \tan^2(\theta_2) & \cdots & \tan^M(\theta_2) \end{bmatrix} \times \begin{bmatrix} \hat{b}_0 \\ \hat{b}_1 \\ \vdots \\ \hat{b}_M \end{bmatrix} = \begin{bmatrix} \omega_{12c}(\theta_1) \\ \omega_{12c}(\theta_1+1) \\ \vdots \\ \omega_{12c}(\theta_2) \end{bmatrix} \tag{35}$$

where the parameters $\omega_{12c}(\theta)$ are determined by the technique in Section II.B when θ varies from θ_1 to θ_2. Once (34) is found, the coefficients in (33) can be determined by solving the least-squares approximation with the objective error function as

$$e(r_{11}(p)) = \int_{p_1}^{p_2} \int_{c(p)} \left\{ \cos(\omega_{12}(p)) - \frac{1}{2}\cos(\omega_1) - \frac{1}{2}\cos(\omega_2) - r_{11}(p)[\cos(\omega_1)\cos(\omega_2) - 1] \right\}^2 dl dp \tag{36}$$

where $\int_{c(p)} \cdot dl$ denotes a line integral along the circular contour

$$c(p) : \omega_1^2 + \omega_2^2 = \begin{cases} \pi^2 & \text{if } p = \tan(\theta) \le 1 \\ (\pi/p)^2 & \text{otherwise.} \end{cases} \tag{37}$$

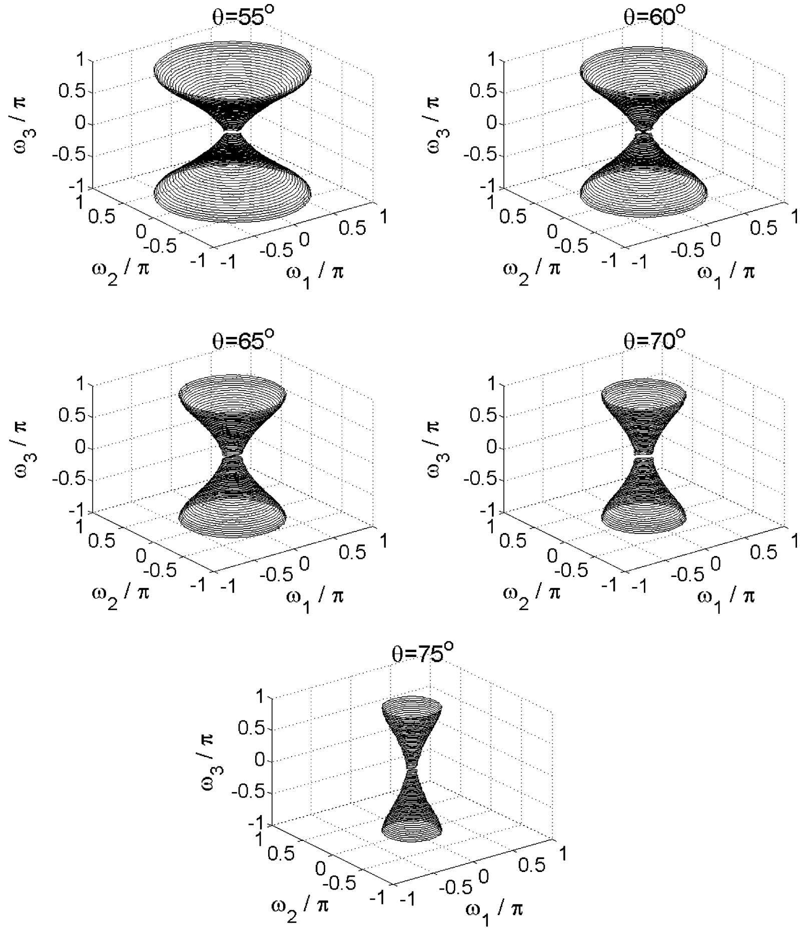

(g)

Fig. 8. *(Continued)* Design of a 3-D FIR variable cone-shaped filter with $\theta_1 = 55°, \theta_2 = 75°, M = 5$ and $N = 20$.(g) Isopotential surfaces at magnitude 0.98 for $\theta = 55°, 60°, 65°, 70°$, and $75°$.

For example, when $M = 5, \theta_1 = 55°, \theta_2 = 75°$, the orbit of $\omega_{12}(p)$ is shown in Fig. 8(d) accompanying the values of $\omega_{12c}(\theta_1), \omega_{12c}(\theta_1 + 1), \ldots, \omega_{12c}(\theta_2)$ marked by "$\circ$", and the isopotential circular cutoff edge contours for different integer inclination degrees are shown in Fig. 8(e).

C. Derivation of the Filter Coefficients for the 3-D Variable Cone-Shaped Filter

Once the coefficients in (30) are determined, the impulse response of the variable transformation subfilter can be computed by (27) and (28), and then the filter coefficients can be obtained in a similar manner as in Section II.D for a specified p. Following the presented examples in Section III-A and III-B, Fig. 8(g) presents the isopotential surfaces at magnitude 0.98 for $\theta = 55°, 60°, 65°, 70°$ and $75°$. For the specified inclination $\theta = 70°$, Fig. 8(f) shows the magnitude responses for $\omega_3 = \pi, 0.75\pi, 0.5\pi$ and 0.25π. To evaluate the performance of the proposed method, the root-mean- squared deviation error of the variable cutoff isopotential is defined by

$$
\begin{aligned}
\varepsilon_{\rm rms} = \Bigg\{ &\frac{1}{(N_p+1)(N_3+1)(N_{12}+1)} \\
&\times \sum_{n_p=0}^{N_p} \sum_{n_3=0}^{N_3} \sum_{n_{12}=0}^{N_{12}} [\cos(\omega_c(p)) \\
&- F(\omega_1, \omega_2, \omega_3, p)]^2 \Bigg\}^{\frac{1}{2}} \\
p &= \tan\left(\frac{n_p(\theta_2-\theta_1)}{N_p} + \theta_1\right) \\
\omega_3 &= \begin{cases} n_3\pi/N_3, & \text{for } p \ge 1 \\ n_3\pi p/N_3, & \text{for } p < 1 \end{cases} \\
\omega_1 &= \frac{\omega_3}{p}\cos\left(\frac{n_{12}\pi}{2N_{12}}\right) \\
\omega_2 &= \frac{\omega_3}{p}\sin\left(\frac{n_{12}\pi}{2N_{12}}\right)
\end{aligned} \tag{38}
$$

which is equal to 0.04302546 when $\theta_1 = 55°, \theta_2 = 75°, N_p = 60$ and $N_3 = N_{12} = 90$. In (38), $F(\omega_1, \omega_2, \omega_3, p)$ denotes the frequency response of variable transformation subfilter for a specified p. The design took 9.218 s of CPU time when $\Delta = \pi/10^3$ is used to find the values marked by "$\circ$" in Fig. 8(a) and (d). Also the scaling problem can be avoided by incorporating the constraints of (12) and (16) in the design procedures. Although, the theoretical proof cannot be given to show this

TABLE II
RELATED COEFFICIENTS FOR THE DESIGN OF A 3-D FIR VARIABLE CONE-SHAPED FILTER WITH $55^\circ \le \theta \le 75^\circ$

Coefficients	$m=0$	$m=1$	$m=2$	$m=3$	$m=4$	$m=5$
b_m	3.54131718	-3.26143631	1.62146579	-0.44891413	0.06503912	-0.00383783
$t(1,1,m)$	-0.75211807	1.37154715	-0.77082135	0.2254595	-0.03335305	0.00196532
$t(0,1,m)$	-0.89145068	0.65088893	-0.36544717	0.11473637	-0.01926224	0.00134384
$\hat{b}_m$	6.99863194	-7.5101446	4.24623083	-1.32737863	0.21700282	-0.01447988
$r(1,1,m)$	1.17578052	-1.49610493	1.02796881	-0.3600674	0.06305512	-0.00436979

fact, but exhaustive simulations show that the frequency responses of (27) for $\omega_i \in [-\pi, \pi]$, $i = 1, 2, 3$ always locate inside $[-1, 1]$.

IV. CONCLUSION

In this paper, a new method has been successfully proposed for the design of 3-D FIR cone-shaped filters. Following the design of a transformation subfilter with fan-type contours, an embedded transformation subfilter is designed to replace one cosine term of the original transformation subfilter. In this paper, the proposed method has also been extended to the design of variable cone-shaped filters, which fully demonstrates the effectiveness and flexibility of the proposed method.

ACKNOWLEDGMENT

The authors would like to thank the anonymous reviewers for their constructive comments on this paper.

REFERENCES

[1] L. T. Bruton and N. R. Bartley, "The design of highly selective adaptive three-dimensional recursive cone filters," *IEEE Trans. Circuits Syst.*, vol. 34, no. 7, pp. 775–781, Jul. 1987.

[2] M. E. Zervakis and A. N. Venetsanopoulos, "Design of three-dimensional digital filters using two-dimensional rotated filters," *IEEE Trans. Circuits Syst.*, vol. 34, no. 12, pp. 1452–1469, Dec. 1987.

[3] A. C. Tan and H. Sun, "Structurally passive synthesis of three- dimensional recursive cone filters," in *Proc. 32nd IEEE Midwest Symp. Circuits Syst.*, Aug. 14–16, 1989, vol. 2, pp. 1119–1122.

[4] M. Bolle, "A closed form design method for recursive 3-d cone filters," in *Proc. IEEE Int. Conf. Acoustics, Speech, Signal Process.*, Apr. 19–22, 1994, vol. 6, pp. 141–144.

[5] G. Runze and P. Steffen, "A contribution to the design of digital three-dimensional FIR and IIR cone filters," in *Proc. 3-D Image Analysis Synthesis*, Nov. 1996, pp. 179–182.

[6] G. Runze, "Efficient design of digital 3-D cone-shaped FIR fan filters using transformations," in *Proc. 10th IEEE Workshop Image Multidimensional Signal Process.*, July 1998, pp. 263–266.

[7] L. T. Bruton, "Selective filtering of spatio-temporal plane waves using 3-D cone filter banks," in *Proc. 2001 IEEE Pacific Rim Conf. Commun. Signal Process. (PACRIM)*, Aug. 26-28, 2001, pp. 67–70.

[8] L. T. Bruton, "Three-dimensional cone filter banks," *IEEE Trans. Circuits Syst. I, Fundam. Theory Appl.*, vol. 50, no. 2, pp. 208–216, Feb. 2003.

[9] L. T. Bruton, "A 3D polyphase-DFT cone filter bank for broad band plane wave filtering," in *Proc. ISCAS*, 2004, pp. III/181–III/184.

[10] B. Kuenzle and L. T. Bruton, "A novel low-complexity spatio-temporal ultra wide-angle polyphase cone filter bank applied to sub-pixel motion discrimination," in *Proc. ISCAS*, 2005, pp. III/2397–III/2400.

[11] S. Singh and D. A. L. Piriyakumar, "Non-uniform bandwidth 3D cone filter bank," in *Proc. 50th Midwest Symp. Circuits Syst.*, Aug. 5–8, 2007, pp. 586–589.

[12] G. Mollova and W. F. G. Mecklenbräuker, "McClellan based design approach for 3-D digital filters with minimization of the integral squared error," *International Journal of Mathematics and Computers in Simulation*, vol. 1, no. 1, pp. 18–25, 2007.

[13] G. Mollova and W. F. G. Mecklenbräuker, "Three-dimensional cone FIR filters design using the McClellan transform," in *Proc. 41st Asilomar Conf. Signals, Syst., Comput.*, Pacific Grove, CA, Nov. 4–7, 2007, pp. 1116–1120.

[14] S. Singh and M. Celenk, "Shaped adaptive three dimensional cone filter bank," in *Proc. 51th Midwest Symp. Circuits Syst.*, Aug. 10–13, 2008, pp. 241–244.

[15] G. Mollova and W. F. G. Mecklenbräuker, "A design method for 3-D FIR cone-shaped filters based on the McClellan transformation," *IEEE Trans. Signal Process.*, vol. 57, no. 2, pp. 551–564, Feb. 2009.

[16] J. H. McClellan, "The design of two-dimensional digital filters by transformations," in *Proc. 7th Ann. Princeton Conf. Information Sci.*, 1973, pp. 247–251.

[17] R. M. Mersereau, W. F. G. Mecklenbräuker, and T. F. Quatieri, JR., "McClellan transformations for 2-D digital filtering: I—design," *IEEE Trans. Circuits Syst.*, vol. 23, no. 7, pp. 405–414, July 1976.

[18] W. F. G. Mecklenbräuker and R. M. Mersereau, "McClellan transformations for 2-D digital filtering: II—Implementation," *IEEE Trans. Circuits Syst.*, vol. 23, no. 7, pp. 414–422, July 1976.

[19] J. H. McClellan and D. S. K. Chan, "A 2D FIR filter structure derived from the Chebyshev recursion,," *IEEE Trans. Circuits Syst.*, vol. CAS-24, no. 7, pp. 372–378, Jul. 1977.

[20] D. T. Nguyen and M. N. S. Swamy, "Approximation design of 2-D digital filters with elliptical magnitude response of arbitrary orientation," *IEEE Trans. Circuits Syst.*, vol. CAS-33, no. 6, pp. 597–603, Jun. 1986.

[21] M. S. Reddy and S. N. Hazra, "Design of elliptically symmetric 2-D FIR filters with arbitrary orientation," *Electronics Lett.*, vol. 23, no. 18, pp. 964–966, Aug. 1987.

[22] E. Z. Psarakis, V. G. Mertzios, and G. P. Alexiou, "Design of two dimensional zero phase FIR fan filters via the McClellan transform," *IEEE Trans. Circuits Syst.*, vol. 37, no. 1, pp. 10–16, Jan. 1990.

[23] S.-C. Pei and J.-J. Shyu, "Design of 2-D FIR digital filters by McClellan transformation and least squares eigencontour mapping," *IEEE Trans. Circuits Syst. II, Analog Digit. Signal Process.*, vol. 40, no. 9, pp. 546–555, Sep. 1993.

[24] C. K. Chen and J. H. Lee, "McClellan transform based design techniques for two-dimensional linear phase filters," *IEEE Trans. Circuits Syst. I, Fundam. Theory Appl.*, vol. 41, no. 8, pp. 505–517, Aug. 1994.

[25] G. V. Moustakides and E. Z. Psarakis, "Design of N-dimensional hyperquadrantally symmetric FIR filters using the McClellan transform," *IEEE Trans. Circuits Syst. II, Analog Digit. Signal Process.*, vol. 42, no. 8, pp. 547–550, Aug. 1995.

[26] Y.-S. Song and Y. H. Lee, "Formulas for McClellan transform parameters in designing 2-D zero-phase FIR fan filters," *IEEE Signal Process. Lett.*, vol. 3, no. 11, pp. 291–293, Nov. 1996.

[27] S.-C. Pei and J.-J. Shyu, "Design of 2-D FIR digital filters by McClellan transformation and least-squares contour mapping," *Signal Process.*, vol. 44, no. 1, pp. 19–26, June 1995.

[28] H. C. Lu and K. H. Yeh, "Optimal design of 2-D FIR digital filters by scaling-free McClellan transformation using least-squares estimation,," *Signal Process.*, vol. 58, no. 3, pp. 303–308, May 1997.

[29] H. C. Lu and K. H. Yeh, "2-D FIR filters design using least squares error with scaling-free McClellan transformation," *IEEE Trans. Circuits Syst. II, Analog Digit. Signal Process.*, vol. 47, no. 10, pp. 1104–1107, Oct. 2000.

[30] C.-C. Tseng, "Design of 2-D FIR digital filters by McClellan transform and quadratic programming," *Proc. Inst. Elect. Eng. Vis. Image Signal Process.*, vol. 148, no. 5, pp. 325–331, Oct. 2001.
[31] C. W. Farrow, "A continuously variable digital delay element," in *Proc. ISCAS*, 1988, pp. 2641–2645.
[32] T.-B. Deng, "Design of linear phase variable 2-D digital filters using real- complex decomposition," *IEEE Trans. Circuits Syst. II, Analog Digit. Signal Process.*, vol. 45, no. 3, pp. 330–339, Mar. 1998.
[33] T.-B. Deng, "Variable 2-D FIR digital filter design and parallel implementation," *IEEE Trans. Circuits Syst. II, Analog Digit. Signal Process.*, vol. 46, no. 5, pp. 631–635, May 1999.
[34] W.-S. Lu and T.-B. Deng, "An improved weighted least-squares design for variable fractional delay FIR filters," *IEEE Trans. Circuits Syst. II, Analog Digit. Signal Process.*, vol. 46, no. 8, pp. 1035–1040, Aug. 1999.
[35] T.-B. Deng and W.-S. Lu, "Weighted least-squares method for designing variable fractional delay 2-D FIR digital filters," *IEEE Trans. Circuits Syst. II, Analog Digit. Signal Process.*, vol. 47, no. 2, pp. 114–124, Feb. 2000.
[36] T.-B. Deng, "Design of linear-phase variable 2-D digital filters using matrix-array decomposition," *IEEE Trans. Circuits Syst. II, Analog Digit. Signal Process.*, vol. 50, no. 6, pp. 267–277, June 2003.
[37] H. H. Dam, A. Cantoni, K. L. Teo, and S. Nordholm, "Variable digital filter with least-square criterion and peak gain constraints," *IEEE Trans. Circuits Syst. II, Exp. Briefs*, vol. 54, no. 1, pp. 24–28, Jan. 2007.
[38] H. H. Dam, A. Cantoni, K. L. Teo, and S. Nordholm, "FIR variable digital filter with signed power-of-two coefficients," *IEEE Trans. Circuits Syst. I, Reg. Papers*, vol. 54, no. 6, pp. 1348–1357, June 2007.
[39] T.-B. Deng and Y. Lian, "Weighted-least-squares design of variable fractional-delay FIR filters using coefficient symmetry," *IEEE Trans. Signal Process.*, vol. 54, no. 8, pp. 3023–3038, Aug. 2006.
[40] C. K. S. Pun, S. C. Chan, and K. L. Ho, "Efficient 1D and circular symmetric 2D FIR filters with variable cutoff frequencies using the Farrow structure and multiplier-block," in *Proc. ISCAS*, 2001, pp. 561–564.
[41] K. S. Yeung and S. C. Chan, "Design and implementation of multiplierless tunable 2-D FIR filters using McClellan transformation," in *Proc. ISCAS*, 2002, pp. 761–764.
[42] J.-J. Shyu, S.-C. Pei, and Y.-D. Huang, "Design of variable 2-D FIR digital filters by McClellan transformation," *IEEE Trans. Circuits Syst. I, Reg. Papers*, vol. 56, no. 3, pp. 574–582, Mar. 2009.
[43] J. H. McClellan, T. W. Parks, and L. R. Rabiner, "A computer program for designing optimum FIR linear phase digital filters," *IEEE Trans. Audio Electroacoust.*, vol. AU-21, no. 6, pp. 506–526, Dec. 1973.
[44] S. J. Leon, *Linear Algebra With Applications*, 7th ed. Englewood Cliffs, NJ: Prentice Hall, 2006.

Jong-Jy Shyu (S'88, M'93, M'06) was born in Taiwan, ROC on March 7, 1960. He received the B.S. degree from Tatung University, Taipei, Taiwan, in 1983 and the M.S. and Ph.D. degrees from National Taiwan University, Taipei, Taiwan in 1988 and 1992, respectively, all in electrical engineering.

In 1992, he joined the department of Computer Science and Engineering, Tatung University as an Associate Professor, and has been a Professor since 1996. From 1997 to 2000, he joined the Department of Computer and Communication Engineering, National Kaohsiung First University of Science and Technology, Kaohsiung, Taiwan, and is currently with the Department of Electrical Engineering, National University of Kaohsiung, Kaohsiung, Taiwan. His research interests include the design and implementation of digital filters, and digital signal processing.

Soo-Chang Pei (SM'89–F'00) was born in Soo-Auo, Taiwan in 1949. He received B.S.E.E. from National Taiwan University in 1970 and M.S.E.E. and Ph.D. degrees from the University of California, Santa Barbara, in 1972 and 1975, respectively.

He was an engineering officer in the Chinese Navy Shipyard from 1970 to 1971. From 1971 to 1975, he was a research assistant at the University of California, Santa Barbara. He was the Professor and Chairman in the Electrical Engineering department of Tatung Institute of Technology and National Taiwan University, from 1981 to 1983 and 1995 to 1998, respectively. Presently, he is the Dean of Electrical Engineering and Computer Science College and the Professor of Electrical Engineering department at National Taiwan University. His research interests include digital signal processing, image processing, optical information processing, and laser holography.

Dr. Pei received National Sun Yet-Sen Academic Achievement Award in Engineering in 1984, the Distinguished Research Award from the National Science Council from 1990–1998, outstanding Electrical Engineering Professor Award from the Chinese Institute of Electrical Engineering in 1998; and the Academic Achievement Award in Engineering from the Ministry of Education in 1998, the Pan Wen-Yuan Distinguished Research Award in 2002, and the National Chair Professor Award from Ministry of Education in 2002. He has been President of the Chinese Image Processing and Pattern Recognition Society in Taiwan from 1996–1998, and is a member of the IEEE, Eta Kappa Nu and the Optical Society of America. He became an IEEE Fellow in 2000 for contributions to the development of digital eigenfilter design, color image coding and signal compression, and to electrical engineering education in Taiwan.

Yun-Da Huang received the B.S. and M.S. degree in electrical engineering from National University of Kaohsiung, Taiwan, in 2006 and 2008, respectively. He is currently working toward the Ph.D. degree in the Graduate Institute of Communication Engineering, National Taiwan University.

His research interests include filter design and digital signal processing.